nature COMMUNICATIONS

ARTICLE

Received 15 Aug 2013 | Accepted 17 Dec 2013 | Published 20 Jan 2014

DOI: 10.1038/ncomms4131

Harnessing *Yarrowia lipolytica* lipogenesis to create a platform for lipid and biofuel production

John Blazeck[1,*], Andrew Hill[1,*], Leqian Liu[1,*], Rebecca Knight[2], Jarrett Miller[1], Anny Pan[1], Peter Otoupal[1] & Hal S. Alper[1,3]

Economic feasibility of biosynthetic fuel and chemical production hinges upon harnessing metabolism to achieve high titre and yield. Here we report a thorough genotypic and phenotypic optimization of an oleaginous organism to create a strain with significant lipogenesis capability. Specifically, we rewire *Yarrowia lipolytica*'s native metabolism for superior *de novo* lipogenesis by coupling combinatorial multiplexing of lipogenesis targets with phenotypic induction. We further complete direct conversion of lipid content into biodiesel. Tri-level metabolic control results in saturated cells containing upwards of 90% lipid content and titres exceeding 25 g l^{-1} lipids, which represents a 60-fold improvement over parental strain and conditions. Through this rewiring effort, we advance fundamental understanding of lipogenesis, demonstrate non-canonical environmental and intracellular stimuli and uncouple lipogenesis from nitrogen starvation. The high titres and carbon-source independent nature of this lipogenesis in *Y. lipolytica* highlight the potential of this organism as a platform for efficient oleochemical production.

[1] McKetta Department of Chemical Engineering, The University of Texas at Austin, 200 E Dean Keeton St. Stop C0400, Austin, Texas 78712, USA. [2] Section of Molecular, Cell and Developmental Biology, The University of Texas at Austin, 1 University Station Stop A6700, Austin, Texas 78712, USA. [3] Institute for Cellular and Molecular Biology, The University of Texas at Austin, 2500 Speedway Avenue, Austin, Texas 78712, USA. * These authors contributed equally to this work. Correspondence and requests for materials should be addressed to H.S.A. (email: halper@che.utexas.edu).

Microbial biosynthesis of fuels (such as ethanol and biodiesel) and industrial chemical precursors provides a renewable means to reduce dependence on petroleum feedstock[1–5]. In particular, bio-based production of oils and lipids provides a unique platform for the sustainable production of biodiesel and other important oleochemicals[5,6]. Most efforts for developing such a platform involve either rewiring *E. coli* or cultivating cyanobacteria. These attempts suffer from low titres ($<7\,g\,l^{-1}$) and variable lipid content (ranging between 10 and 87%), with the highest of these levels typically occurring in non-tractable, slow-growing hosts cultivated in oil-containing media (that is, *ex novo* lipid incorporation instead of *de novo* lipogenesis)[3,5,7–11].

As an alternative, several groups have explored oleaginous organisms such as the fungus *Yarrowia lipolytica*, but total oil content and titres are still limited[12–17]. Yet, the genetic tractability of *Y. lipolytica*[18–24] coupled with its modest, innate *de novo* lipogenesis ($\sim$10–15% lipid content in wild type[13,14,25–27]) make it a potential candidate as a platform organism for superior lipid production.

Lipid biosynthesis is primarily initiated by the activity of four enzymes—AMP deaminase (AMPD), ATP-citrate lyase (ACL), malic enzyme (MAE) and acetyl-CoA carboxylase (ACC)—that cooperatively divert carbon flux from central carbon metabolism towards fatty-acid precursors[15,26]. AMPD inhibits citric acid cycle flux to promote the accumulation of citrate, which is then cleaved into acetyl-CoA by ACL. Fatty-acid synthesis is further encouraged by carboxylation of acetyl-CoA to malonyl-CoA fatty-acid building blocks by ACC and by an increased NADPH supply generated by MAE or the pentose phosphate pathway[15,26,28] (Fig. 1a). Leucine biosynthetic capacity has also been implicated as an effector of lipogenic ability in oleaginous organisms[25,29], and a putative acetyl-CoA-generating leucine degradation pathway was recently identified through a comparative genomics analysis of non-oleaginous and oleaginous yeast strains[30]. In this regard, *Y. lipolytica* also possesses homologues for every enzyme and enzymatic subunit necessary for acetyl-CoA generation through isoleucine degradation (>45% similarity to *Homo sapiens* enzymes)[31,32]. Previous efforts to increase lipid accumulation have shown promise in *Y. lipolytica*. In particular, deletion of β-oxidation enzymes coupled with enhancing glycerol synthesis substantially increased *ex novo* lipid accumulation[15,26] and deletion of the *pex10* peroxisomal biogenesis gene greatly increased eicosapentaenoic acid yields[33]. However, these studies have been limited by their breadth of metabolic control and their comprehensiveness of genotypic and phenotypic sampling towards complete redirection of metabolic flux towards lipid accumulation[13–15,25]. Moreover, *de novo* lipid content in this organism has been limited to below $\sim$60% by dry cell weight[13].

Here we undertake a large-scale engineering effort—multiplexing genomic engineering of lipogenesis targets with phenotypic induction—and create a *Y. lipolytica* strain with significantly improved lipogenesis capability. Simultaneous perturbation of five lipogenic targets (affecting three disparate metabolic pathways) results in lipid-saturated cells, culminating in the highest reported lipid content ($\sim$90%) and lipid titre ($25.3\,g\,l^{-1}$) to date. The latter milestone represents a >60-fold improvement over parental strain and conditions. Through this rewiring effort, we describe several non-canonical facets of lipogenesis, including that lipogenesis is dependent on absolute environmental carbon content, that rare odd-chain fatty-acid pathways are naturally activated by high lipogenesis, that lipid accumulation phenotypes are dependent on leucine-mediated signalling and that high lipogenesis can be uncoupled from nitrogen starvation and entails a reduction in citric acid cycling. We further demonstrate that these lipids can be easily converted into fatty acid methyl esters (FAMEs) suitable for biodiesel. This work demonstrates, and capitalizes upon, the lipogenic potential of *Y. lipolytica*, utilizing its amenable metabolism to realize high titres and carbon-source independent lipid accumulation.

Results

Combinatorial genomic rewiring for improved lipogenesis. In this work, we investigate a combinatorial multiplexing of targets spanning fatty acid, lipid and central metabolism through the overexpression of five lipogenesis enzymes in four genomic backgrounds marked by differential fatty acid catabolic capacity (Table 1, Fig. 1a). Specifically, AMPDp, ACLp, and MAEp overexpression were investigated for their potential to increase acetyl-CoA and NADPH supply (ACCp overexpression has not been reported to significantly improve lipogenesis and was excluded[13]) and DGA1p and DGA2p (acyl-CoA:diacylglycerol acyltransferases isozymes I and II) were included for their potential in catalysing the ultimate step in triglyceride synthesis[34]. These overexpression targets were multiplexed with deletions that served to reduce fatty-acid catabolism by reducing one or both of β–oxidation (via *mfe1* deletion)[14,15] and peroxisome biogenesis (via *pex10* deletion)[25,35] (Table 1). We have previously demonstrated that restoration of a complete leucine biosynthetic pathway increased lipid accumulation more than alleviation of uracil auxotrophy in a PO1f base strain[25]. Thus, we included the complementing of leucine and uracil biosynthetic capacity both singly and in tandem as targets for this multiplexing. Integrated expression cassettes were driven by our high-strength synthetic $UAS1B_{16}$-TEF constitutive hybrid promoter[23]. Collectively, the combinatorial multiplexing of enzyme overexpressions, fatty-acid inhibition knockouts and other biosynthetic pathways resulted in 57 distinct genotypes that were analysed for lipogenesis capacity compared with the wild-type strain (Supplementary Table 1). Initially, a nile red-based fluorescence assay coupled with flow cytometry[36] was used to efficiently determine relative lipid content and assess critical genotype synergies. Across the resulting lipogenesis metabolic landscape, we observed a significant range in lipid accumulation that spanned a 74-fold improvement in fluorescence over unmodified *Y. lipolytica* PO1f (Fig. 1b). Using fluorescence microscopy, it is evident that cells become larger and visibly more saturated with lipid content across the resulting lipogenic continuum in this landscape (Fig. 1c).

Three dominant genetic targets exhibited cooperativity towards enhancing lipogenesis—*pex10* deletion, DGA1p or DGA2p overexpression and restoration of a complete leucine biosynthetic pathway (leucine$^+$ genotype) (Fig. 1b). Each of these targets independently improved nile red-based fluorescence by more than threefold, and DGA1p overexpression outperformed that of DGA2p (Fig. 1b, Supplementary Figs 1–3). Overexpression of MAE and AMPD were positive effectors of lipogenesis, but offered no cooperative advantage when combined into the *pex10* leucine$^+$ DGA1p overexpression background, potentially by unbalancing metabolic flux towards lipid production through the overproduction of fatty-acid synthesis precursors (Fig. 1b). Deletion of the *mfe1* gene was not seen to alter total nile red-based lipid fluorescence measurements, but its removal reduces fatty-acid degradation in carbon starvation conditions[15,25]. Similarly, the uracil$^+$ genotype had minimal effect on fluorescence, but improved growth rate and permitted cultivation in a pure minimal medium composition. Thus, the *pex10*, *mfe1*, leucine$^+$, uracil$^+$, DGA1p overexpression genotype, the strain with the highest lipogenesis potential in terms of fluorescence, was selected as our most advantageous strain. We extracted and

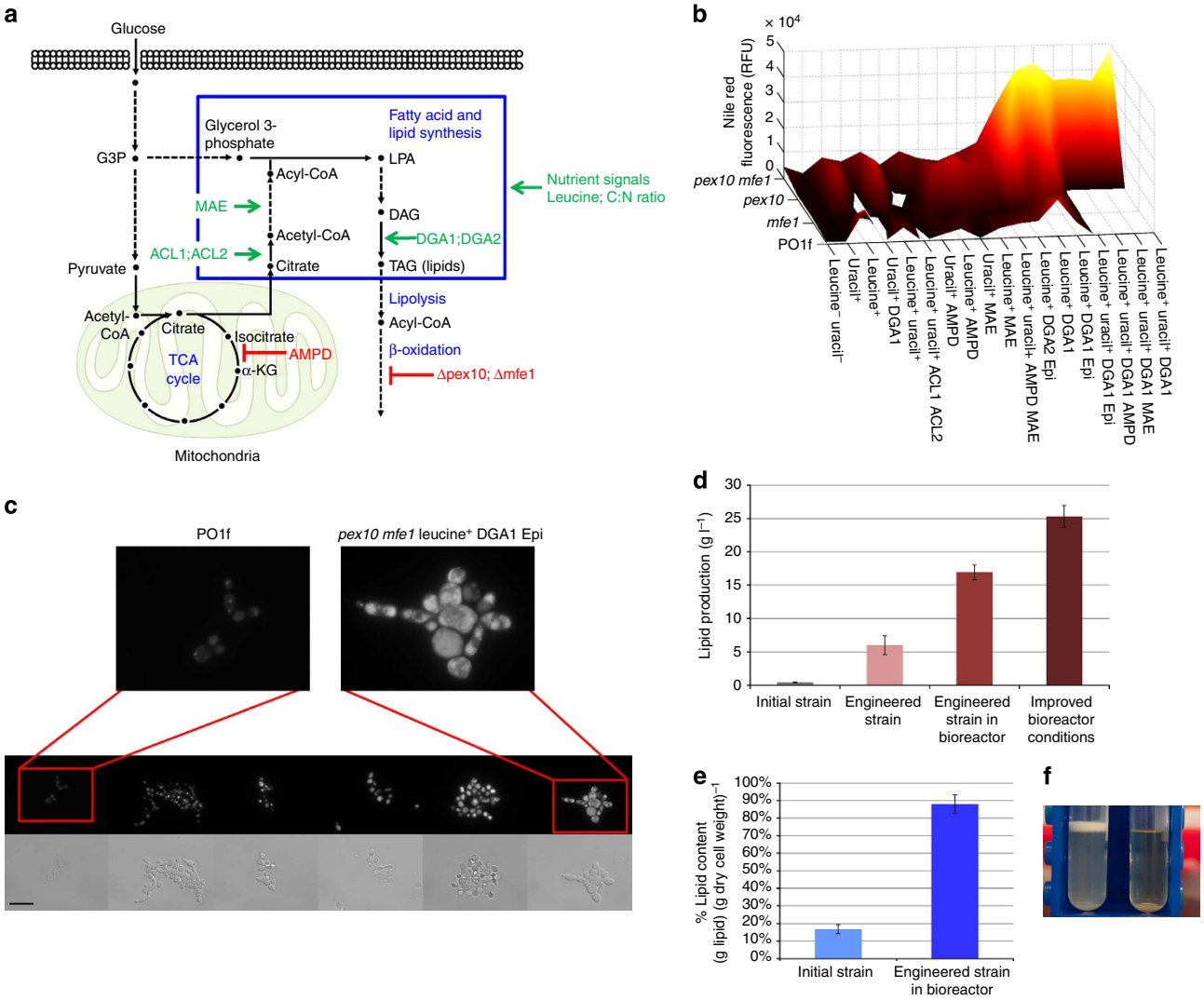

Figure 1 | Combinatorial strain engineering. (**a**) A schematic illustrating the pathways rewired in *Y. lipolytica's* metabolism to drastically increase lipogenesis capacity. (**b**) Nile red fluorescence analysis of the strains constructed in this study. Strain names include strain background (POIf, *pex10, mfe1, pex10 mfe1*), auxotrophies relieved (leucine$^+$ or uracil$^+$) and enzymes overexpressed. 'Epi' denotes episomal overexpressions. Lipogenesis is induced as *pex10* deletion is coupled with leucine biosynthetic capacity and DGA1 overexpression—generally from front left to back right of the 3D contour heat map representation. Error bars represent the s.d of technical triplicates.(**c**) Fluorescence light microscopy images of six strains increasing in lipid content (white) from left (unmodified POIf) to right (*pex10 mfe1* leucine$^+$ DGA1). Scale bar, 20 μm. (**d**,**e**) Increases in lipid titre and lipid content realized by engineering POIf to create the *pex10 mfe1* leucine$^+$ uracil$^+$ DGA1 strain and then optimizing fermentation conditions in a bioreactor. Error bars represent s.d. of technical triplicates. (**f**) Image of lysed *pex10 mfe1* leucine$^+$ uracil$^+$ DGA1 (left) and POIf control (right) cells in 14ml culture tubes. Lipids remain floating after centrifugation.

measured lipid content to confirm nile red-based flow cytometry assessment of lipid content (Fig. 1d–f and Supplementary Figs 4 and 5). In small-scale test-tube cultivations, the final engineered strain outperformed all others, yielding 6.00 g l^{-1} lipids with 74% lipid content, a ~15-fold improvement over control (0.41 g l^{-1} lipid and 16.8% lipid content).

Lipogenic induction through nutrient level optimization. We next sought to understand the complex relationship between *de novo* lipid accumulation and nutrient levels. Prior to this study, it was generally accepted that lipogenesis capacity is highly dependent on the ratio of available carbon and nitrogen (C:N ratio) and that lipogenesis induction requires a nitrogen starvation mechanism[27,37]. However, no definitive, quantitative relationship between genotype and lipogenesis induction has been determined. Thus, we analysed the effect of nitrogen starvation and carbon availability on lipogenesis for unmodified *Y. lipolytica* PO1f and 11 engineered strains spanning the lipogenesis landscape (Supplementary Table 2). Cultivation of these 12 strains in 13 media formulations containing between 10 and 160 g l^{-1} glucose and 0.055 and 1.365 g l^{-1} ammonium revealed that absolute glucose level, rather than generally accepted C:N ratio, is crucial towards inducing lipid synthesis, and high-lipid producers realized optimal accumulation in higher glucose media (Fig. 2, Supplementary Table 3, Supplementary Figs 6–14). In particular, unmodified *Y. lipolytica* PO1f and other low-performing strains were most strongly induced by a lower carbon level (20 g l^{-1} glucose and 0.273 g l^{-1} ammonium), but responded poorly at similar C:N ratios with higher glucose and ammonium concentrations (Fig. 2a, Supplementary Figs 6–8). Moderate lipid accumulators were highly induced at intermediate glucose levels but again responded poorly at similar C:N ratios (Fig. 2b, Supplementary Figs 9–12). The highest accumulators, including the *pex10 mfe1* leucine$^+$ DGA1p overexpression

Table 1 | List of genes and enzymes in this study.

Genomic backgrounds

Name	Genotype (function of knockout)
POlf	MatA, leucine$^-$, uracil$^-$, no extracellular proteases
pex10	POlf-Δpex10 (prevents peroxisome biogenesis)
mfe1	POlf-Δmfe1 (prevents β-oxidation)
pex10 mfe1	POlf-Δpex10 Δmfe1 (prevents peroxisome biogenesis and β-oxidation)

Enzymatic overexpressions

Name	Function
AMPD	Inhibits TCA cycle, increasing citric acid level
$ACL_{subunit}1$	Cleaves citric acid to acetyl-CoA
$ACL_{subunit}2$	Cleaves citric acid to acetyl-CoA
MAE	Increases NADPH cofactor supply
$DGA_{isozyme}1$	Catalyses lipid synthesis step
$DGA_{isozyme}2$	Catalyses lipid synthesis step

Auxotrophic markers

Name	Utilized for expression
Leucine$^{+/-}$	Episomally and chromosomally
Uracil$^{+/-}$	Chromosomally

ACL, ATP-citrate lyase; AMPD, adenosine monophosphate deaminase; DGA, acyl-CoA:diacylglycerol acyltransferases; MAE, malic enzyme. ACL is a heterodimeric protein so only dual overexpressions of the $ACL_{subunit}1$ and $ACL_{subunit}2$ were constructed and tested.

genotype, were induced most intensely by higher levels of carbon and nitrogen ($80\,g\,l^{-1}$ glucose and $1.365\,g\,l^{-1}$ ammonium) (Fig. 2c, Supplementary Figs 13 and 14). Thus, the current paradigm asserting the necessity of nitrogen starvation and that similar C:N ratios beget similar induction irrespective of overall carbon and nitrogen levels is incorrect. Instead, a defined amount of carbon content ultimately controls lipid synthesis, and this favourable carbon level increases in strains capable of superior lipogenesis. Increasing carbon and nitrogen levels only improves lipogenesis to a certain extent, as lipid yield decreases when glucose levels are increased to $160\,g\,l^{-1}$ (Fig. 2c), and cultivation of various engineered strains in media containing $320\,g\,l^{-1}$ glucose drastically reduced growth rate, most likely due to osmotic stress[38]. Similar linkages between high carbon content versus caloric restriction may present interesting parallels in other organisms.

Controlled fermentation enables superior lipogenesis. Taken together, these dominant lipogenesis targets and nutrient levels (specifically, $80\,g\,l^{-1}$ glucose and $1.365\,g\,l^{-1}$ ammonium) enabled an optimization of fermentation conditions for the *pex10 mfe1* leucine$^+$ uracil$^+$ DGA1 overexpression strain to maximize lipid accumulation in a bioreactor setting. We cultivated this fully prototrophic strain in an inexpensive minimal media formulation consisting of only glucose, ammonium sulphate and yeast nitrogen base. By additionally controlling pH, temperature and dissolved oxygen levels, we observed significantly improved lipid titre to $16.1\,g\,l^{-1}$ with cells containing up to 88% lipid cellular content, the highest reported yield and content to date (Figs 1d,e and 3a, Supplementary Fig. 15). This represents a 5.4-fold increase over a POlf leucine$^+$ uracil$^+$ control and 63% of the theoretical stoichiometric yield with a specific productivity approaching $0.2\,g\,l^{-1}\,h^{-1}$ (Fig. 3). Lipogenesis continues in the engineered strain throughout the 6-day fermentation despite complete depletion of glucose and cessation of biomass production within 3 days (Fig. 3a). Moreover, this engineered strain exhibits reduced citric acid and biomass production to enable heightened flux towards lipid synthesis (Fig. 3a,c). In contrast, excess carbon flux in the control strain accumulates as citric acid (dispersed throughout the supernatant) before reabsorption and incorporation into biomass (Fig. 3c). Thus, the engineered strain's metabolic processes are in stark contrast to a central tenet of lipid accumulation in oleaginous organisms—that lipid accumulation requires prior production of citric acid[39–41]. We hypothesize that our re-engineered metabolism enables temporary carbon storage in secondary metabolites more amenable to direct incorporation into elongating fatty acids, potentially exclusively intracellular metabolites such as acetyl-CoA or malonyl-CoA.

Doubling nutrient availability to $160\,g\,l^{-1}$ glucose and $2.73\,g\,l^{-1}$ ammonium further increased lipid titre to $25.3\,g\,l^{-1}$, the highest reported titre to date (Fig. 1d, Supplementary Fig. 16). This represents an increase in specific productivity to $0.21\,g\,l^{-1}\,h^{-1}$, but a decrease in cellular lipid content to 71% and a decrease to 44% of theoretical stoichiometric yield. This further demonstrates the need to fully optimize carbon and nitrogen content to maximize lipogenic efficiency. These extremely high lipogenesis levels correlated with a metabolic shift to maintain homoeostatic, steady state ammonium levels not seen in the low lipid accumulation background. (Fig. 3b,d, Supplementary Fig. 16). Specifically, after an initial drop, engineered cells re-buffered the nitrogen level within the media, thus illustrating a newfound, decoupled relationship between lipogenesis and nitrogen starvation. The control and engineered strain both exhibit similar intracellular protein degradation during the final 4 days of fermentation (Supplementary Fig. 17). However, the control strain produces $4.9\,g\,l^{-1}$ biomass containing $\sim$11% nitrogen content (thus utilizing $0.54\,g\,l^{-1}$ nitrogen)[42], while the engineered strain re-buffers supernatant nitrogen levels to $\sim 0.5\,g\,l^{-1}$. A simple mass balance indicates that the nitrogen replenishment afforded by engineered cells is originating from protein degradation. Interestingly, the purely lipogenic phase (after biomass accumulation) in the engineered cells corresponds to a reduction in oxygen utilization, evidenced by a large, prolonged spike in dissolved oxygen content (Supplementary Fig. 18), suggesting that both nitrogen and oxygen utilization are downregulated to reduce metabolite utilization for cell growth to enable enhanced lipogenesis.

High lipogenesis with alternative carbon sources. We further tested this engineered strain on alternative carbon sources to assay for carbon-source independent lipogenesis. We observed that the *pex10 mfe1* leucine$^+$ uracil$^+$ DGA1p overexpression strain exhibited superior production in nearly all carbon sources, establishing these lipogenesis targets as essential in rewiring this organism into an oleochemical platform strain (Fig. 4, Supplementary Fig. 19).

Lipid analysis and conversion into soybean-like biodiesel. We analysed lipid content with GC and saw predominantly C16:0, C16:1, C18:0, C18:1 and C18:2 fatty acids (very similar to soybean), making these lipid reserves ideal feedstock for biodiesel synthesis (Fig. 5, Supplementary Fig. 20)[43]. Moreover, we observed $127\,mg\,l^{-1}$ accumulation of C17 fatty acids, a very rare metabolite in cells (Supplementary Figs 21 and 22). We hypothesize that extremely active lipogenesis enables less-favored odd-chained synthesis and such high titres permit detection and characterization. Finally, a standard methanol transesterification reaction with bioreactor-extracted lipids demonstrated *de novo* biodiesel production (Supplementary Fig. 23). Thus, the microbial production of high lipids in this host can facilitative a renewable biodiesel production process with profiles similar to conventional plant-derived oils.

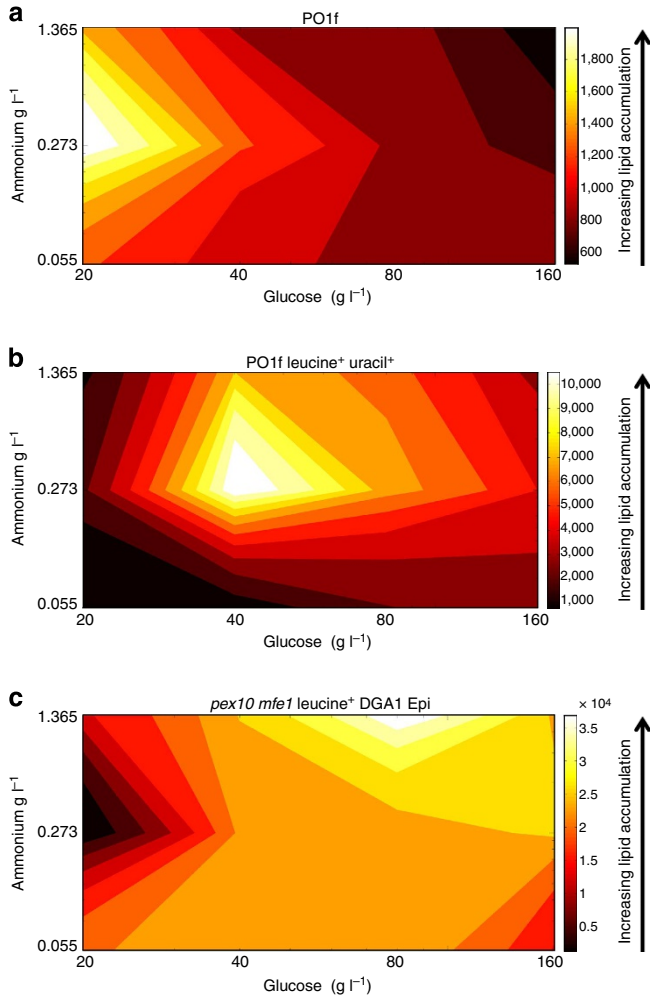

Figure 2 | Genotypic dependency towards lipid induction phenotype. Heat maps of nile red-stained lipid fluorescence for the (**a**) POIf low-lipid-accumulating strain, (**b**) POIf leucine$^+$ uracil$^+$ moderate lipid-accumulating strain, and (**c**) *pex10 mfe1* leucine$^+$ DGA1 high-lipid-accumulating strain demonstrate a decoupling of lipogenesis and nitrogen starvation as well as the implication of absolute carbon content as a lipogenesis effector. Fluorescence data is shown for each strain after cultivation and staining in twelve media formulations containing between 20 g l^{-1} and 160 g l^{-1} glucose and 0.055 g l^{-1} and 1.365 g l^{-1} ammonium. Lipogenesis is dependent on absolute environmental carbon content and low lipid accumulators (**a**) require less carbon for optimal lipogenic induction than moderate (**b**) or high (**c**) lipid accumulating strains. In highly lipogenic strains (**c**), high lipogenesis is uncoupled from nitrogen starvation. These studies were conducted with technical duplicates.

Probing the link between leucine and lipogenesis. Finally, we sought to explain the lipogenic benefit bestowed by leucine biosynthetic capacity by comparing leucine supplementation to genetic complementation. Leucine supplementation mimicked genotypic complementation in leucine$^-$ strains but did not affect leucine$^+$ backgrounds (Fig. 6, Supplementary Fig. 24). Isoleucine supplementation had no effect, ensuring that this leucine-mediated response was not a result of amino-acid catabolism (Fig. 6). Leucine supplementation or genetic complementation enabled a pronounced alteration in steady-state nitrogen concentration that correlated with lipogenesis in small-scale cultivations (Supplementary Figs 25 and 26). These results implicated leucine as an intracellular trigger to stimulate lipogenesis while regulating nitrogen availability. In this regard, the

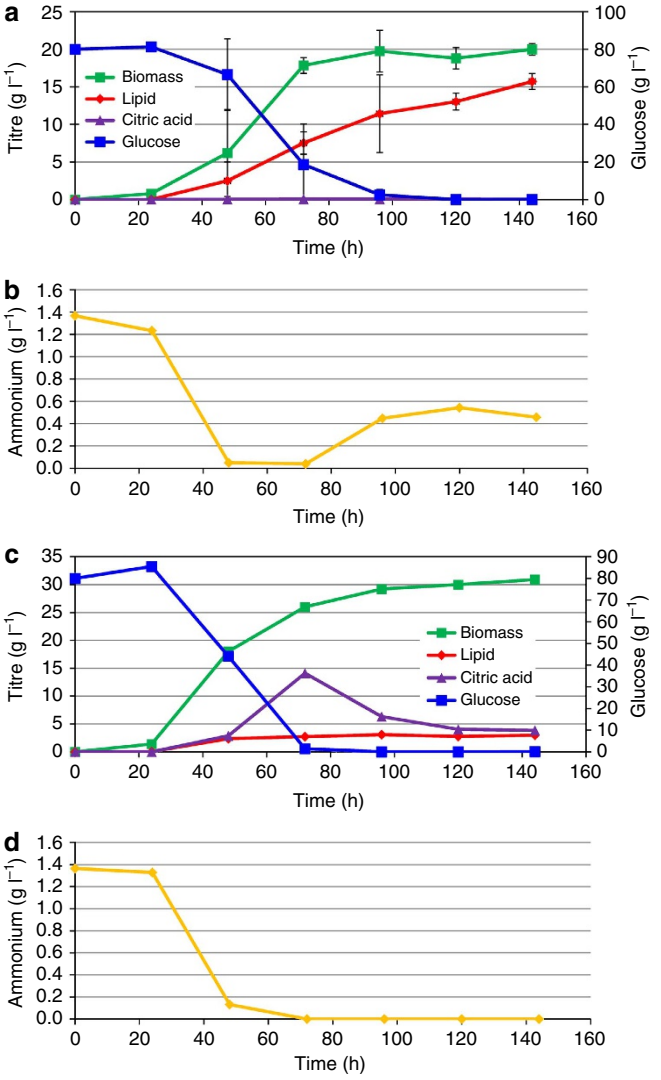

Figure 3 | Fermentation profiles of pex10 mfe1 leucine$^+$ uracil$^+$ DGA1 and POIf leucine$^+$ uracil$^+$. Time courses of the 1.5 l scale batch fermentation of the *pex10 mfe1* leucine$^+$ uracil$^+$ DGA1 (**a**,**b**) and POIf leucine$^+$ uracil$^+$ (**c**,**d**) strains in 80 g l^{-1} glucose, 6.7 g l^{-1} YNB (no amino acids, 1.365 g l^{-1} ammonium) are shown, including production of biomass, lipids and citric acid (left axis **a**,**c**), consumption of glucose (right axis **a**,**c**), and ammonium level (**b**,**d**). (**a**) During the *pex10 mfe1* leucine$^+$ uracil$^+$ DGA1 fermentation, negligible citric acid was produced and lipid product accumulated during and after biomass production phases. This fermentation was run three times in identical conditions, reaching final yields of 15.25 g l^{-1} lipids and 20.3 g l^{-1} biomass (75% lipid content), 14.96 g l^{-1} lipids and 20.6 g l^{-1} biomass (73% lipid content), and 16.9 g l^{-1} lipids and 19.21 g l^{-1} biomass (88% lipid content). Most time points show average values from the former two fermentations (75 and 73% final lipid content), while end-points represent averages from all three final values. Error bars represent s.d. of these technical replicates. Glucose and ammonium substrate were fully consumed after 72 h, but surprisingly, (**b**) ammonium level was replenished to a steady state level of ~0.5 g l^{-1}, ~40% of the original starting level. (**c**) During the POIf leucine$^+$ uracil$^+$ fermentation, citric acid accumulated to more than 14 g l^{-1} after 72 h before quickly reducing to 4 g l^{-1}. Lipid production did not trend with biomass production, reaching a final yield of only 3 g l^{-1} lipids, compared with 30 g l^{-1} biomass and glucose was again consumed within 72 h. (**d**) Ammonium was fully consumed after 72 h with no replenishment as observed in the mutant strain.

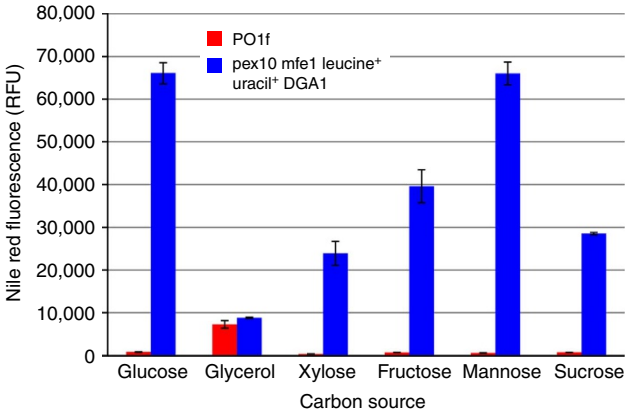

Figure 4 | Lipid accumulation on alternative carbon sources. The *pex10 mfe1* leucine$^+$ uracil$^+$ DGA1 strain effectively generates high lipid content in a carbon-source independent manner. Error bars represent s.d. of biological triplicates.

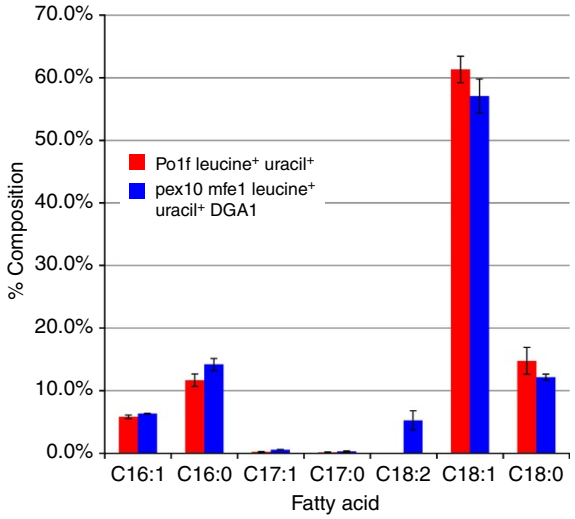

Figure 5 | Fatty-acid profiles following fermentation. Fatty-acid profiles of lipid extract from *pex10 mfe1* leucine$^+$ uracil$^+$ DGA1 and POIf leucine$^+$ uracil$^+$ strains after 6 day bioreactor batch fermentations are shown. We observed predominantly C16 and C18 fatty-acid content, as expected, with a noticeable amount of C17 accumulation. We observed C18:2 (linoleic acid) accumulation in the *pex10 mfe1* leucine$^+$ uracil$^+$ DGA1 but not in the POIf leucine$^+$ uracil$^+$ control. Error bars represent s.d. of technical triplicates.

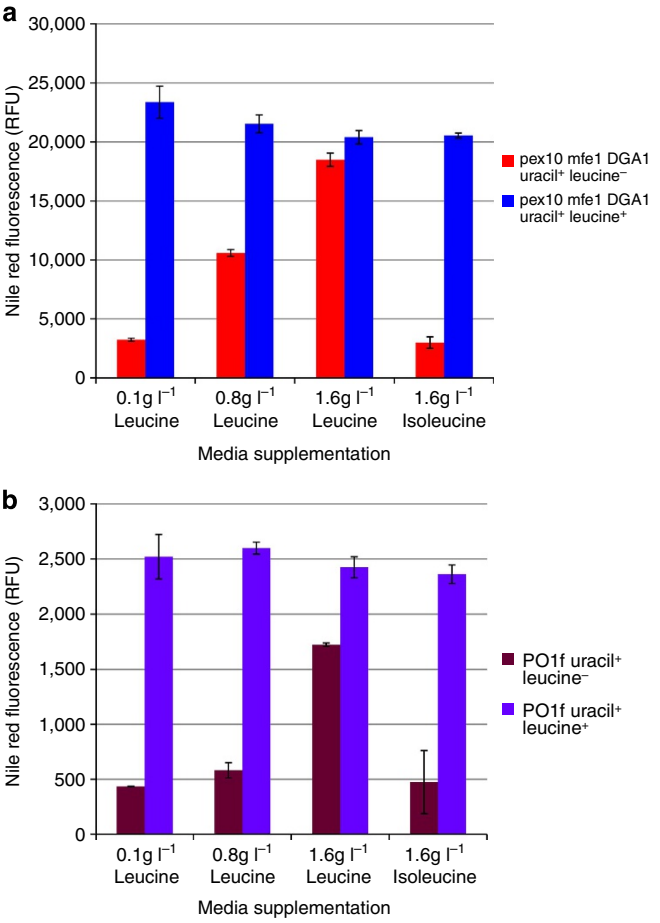

Figure 6 | Leucine supplementation recovers leucine$^+$ phenotype while isoleucine supplementation does not. The ability of leucine or isoleucine supplementation to complement the leucine$^+$ phenotype in the (**a**) *pex10 mfe1* leucine$^-$ uracil$^+$ DGA1 and the (**b**) PO1f leucine$^-$ uracil$^+$ backgrounds was tested. Leucine (1.6 g l^{-1}) supplementation complemented the leucine$^+$ phenotype in both the *pex10 mfe1* leucine$^-$ uracil$^+$ DGA1 and the PO1f leucine$^-$ uracil$^+$ backgrounds. Leucine supplementation had no effect on the *pex10 mfe1* leucine$^+$ uracil$^+$ DGA1 background or the PO1f leucine$^+$ uracil$^+$ backgrounds, demonstrating the leucine biosynthetic capacity generates enough leucine to stimulate lipogenesis. Isoleucine had no effect on lipogenesis in either the leucine$^+$ or leucine$^-$ backgrounds. Thus, the benefit of leucine towards lipogenesis is not a result of leucine catabolism for carbon and nitrogen use. Error bars represent s.d. of biological triplicates.

yeast and mammalian TOR complexes (TORC1) promote cell anabolic processes, such as growth, proliferation and protein synthesis, in response to amino acid availability and growth factor stimuli[44,45]. The leucyl-tRNA synthetase has recently been implicated as an intracellular sensor of amino-acid availability for the TORC1, providing a potential link between leucine stimulation and lipogenesis[46,47]. To probe this interaction further, we inhibited *Y. lipolytica* TOR kinase activity with rapamycin, revealing a complex TOR-regulated lipogenic phenotype, in which leucine stimulation and TOR inhibition coupled to facilitate lipogenesis in low-lipid production backgrounds but reduced lipogenesis in high-production strains (Supplementary Fig. 27). Thus, we demonstrated here that leucine-mediated lipogenic induction is affected by TOR regulation, though not in the mechanism described for protein synthesis.

Discussion

Lipogenic organisms offer ideal platforms for biodiesel and oleochemical synthesis. To this effect, we rewired *Y. lipolytica's* native metabolism via a combinatorial multiplexing to effect superior *de novo* lipid accumulation. Our analyses revealed that high lipogenesis can be uncoupled from nitrogen starvation, is dependent on leucine-mediated signalling and absolute environmental carbon content and is adversely affected by citric acid and nitrogen cycling. For the majority of our moderate or highly lipogenic strains, optimal lipid accumulation was enabled in nitrogen-permissive, high-carbon conditions. In contrast, low-performing strains were optimally induced by low carbon levels, indicating central carbon metabolisms ill-equipped to utilize energy-dense media formulations. Thus, genomic rewiring quickly eliminates the requirement of induction through nitrogen starvation and necessitates a re-optimization of environmental stimulus after each metabolic perturbation. During bioreactor

fermentation, a lowly lipogenic strain diverted excess carbon to the production of extracellular citric acid before assimilation into biomass (simultaneously utilizing nitrogen derived from protein degradation). In contrast, a highly lipogenic strain avoided citric acid accumulation and prevented incorporation of nitrogen into biomass. In this manner, our final engineered strain maintained nitrogen levels optimal for high lipogenesis and prevented extracellular carbon flux, promoting easier lipid accumulation.

We report here on the novel link between leucine signalling and lipogenesis in *Y. lipolytica*. Specifically, we contrasted the effects of leucine and isoleucine supplementation on lipogenesis and demonstrated that only leucine acts to promote lipogenesis. As *Y. lipolytica* possesses degradation pathways for both leucine and isoleucine to acetyl-CoA fatty-acid precursors[30–32], leucine must act as an intracellular signal to permit lipid production, rather than as a carbon source. This is further established by the leucine-dependent TOR-inhibition phenotype of the PO1f leucine$^-$ uracil$^+$ and PO1f leucine$^+$ uracil$^+$ strains (Supplementary Fig. 27). Thus, a complex signalling scheme is implicated for high-lipid titres in this organism.

In summary, we conducted the largest rewiring of an oleaginous organism, and successfully engineered and enhanced *de novo* lipid accumulation in *Y. lipolytica* by >60-fold when compared with the starting strain. In doing so, we identified several unique features of lipogenesis, demonstrated that lipid accumulation approaching 90% of cell mass is possible, determined dominant genotype–phenotype dependencies, de-coupled lipogenesis and nitrogen starvation, illustrated carbon-source independence and demonstrated the feasible conversion of these lipids into FAMEs. We further presented evidence that two central tenets of lipogenesis, the necessity for nitrogen starvation and citric acid cycling, are not universal. This work reports the highest lipid titres to date at 25 g l^{-1} and should serve as a stepping stone towards creating a robust, efficient, high-production platform for ubiquitous conversion of carbon into value-added oleochemical and biofuel products.

Methods

Base strains and media. *E. coli* strain DH10B was used for cloning and plasmid propagation. DH10B was grown at 37 °C with constant shaking in Luria–Bertani Broth (Teknova) supplemented with 50 μg ml^{-1} of ampicillin for plasmid propagation. *Y. lipolytica* strain PO1f (ATCC # MYA-2613), a leucine and uracil auxotroph devoid of any secreted protease activity[48], was used as the base strain for all studies. Supplementary Table 1 contains a complete list of PO1f derivatives produced in this study. *Y. lipolytica* was cultivated at 30 °C unless otherwise stated with constant agitation. Cultures (2 ml) of *Y. lipolytica* used in large-scale screens were grown in a rotary drum (CT-7, New Brunswick Scientific) at speed seven, and larger culture volumes were shaken in flasks at 225 r.p.m. or fermented in a bioreactor.

YSC media consisted of 20 g l^{-1} glucose (Fisher Scientific), 0.79 g l^{-1} CSM supplement (MP Biomedicals) and 6.7 g l^{-1} Yeast Nitrogen Base w/o amino acids (Becton, Dickinson, and Company). YSC-URA, YSC-LEU and YSC-LEU-URA media contained 0.77 g l^{-1} CSM-Uracil, 0.69 g l^{-1} CSM-Leucine or 0.67 g l^{-1} CSM-Leucine-Uracil in place of CSM, respectively. YPD media contained 10 g l^{-1} yeast extract (Fisher Scientific), 20 g l^{-1} peptone (Fisher Scientific) and 20 g l^{-1} glucose, and was often supplemented with 300 μg ml^{-1} Hygromycin B (Invitrogen) for knockout selection. Lipid accumulation response towards media formulation was investigated by cultivation in varying concentrations of glucose and nitrogen. These media formulations contained 0.79 g l^{-1} CSM, 1.7 g l^{-1} Yeast Nitrogen Base w/o amino acid and w/o $(NH_4)_2SO_4$ (Becton, Dickinson, and Company), between 20 g l^{-1} and 160 g l^{-1} glucose, and between 0.2 g l^{-1} and 5 g l^{-1} ammonium sulphate—$(NH_4)_2SO_4$ (Fisher Scientific)—which corresponds to between 0.055 g l^{-1} and 1.365 g l^{-1} ammonium. Minimal media formulations utilized for bioreactor fermentations typically contained 80 g l^{-1} glucose and 6.7 g l^{-1} Yeast Nitrogen Base w/o amino acids (1.7 g l^{-1} YNB and 5 g l^{-1} $(NH_4)_2SO_4$). When utilizing alternative carbon sources, glucose was replaced by 80 g l^{-1} arabinose (Fisher Scientific), 80 g l^{-1} fructose (Alfa Aesar), 80 g l^{-1} galactose (Fisher Scientific), 80 g l^{-1} glycerol (Fisher Scientific), 80 g l^{-1} mannose (Alfa Aesar), 80 g l^{-1} maltose (Acros Organics), 80 g l^{-1} ribose (MP Biomedicals), 80 g l^{-1} sucrose (Acros Organics) or 80 g l^{-1} Xylose (Acros Organics). Solid media for *E. coli* and *Yarrowia lipolytica* was prepared by adding 20 g l^{-1} agar (Teknova) to liquid media formulations. Leucine (MP Biomedicals) and isoleucine (Sigma Aldrich) supplementation was used to analyse the effect of leucine biosynthetic capacity. Leucine was added at a concentration of 0.8 g l^{-1} or 1.6 g l^{-1}, while isoleucine was added at a concentration of 1.6 g l^{-1}. Inhibition of the TOR protein was caused by supplementation with 200 ng ml^{-1} rapamycin (LC Laboratories).

Cloning and transformation procedures. All restriction enzymes were purchased from New England Biolabs and all digestions were performed according to standard protocols. PCR reactions were set up with recommended conditions using Phusion high-fidelity DNA polymerase (Finnzymes) or LongAmp *Taq* DNA polymerase (New England Biolabs). Ligation reactions were performed overnight at room temperature using T4 DNA Ligase (Fermentas). Gel extractions were performed using the Fermentas GeneJET extraction kit purchased from Fisher Thermo Scientific. *E. coli* minipreps were performed using the Zyppy Plasmid Miniprep Kit (Zymo Research Corporation). *E. coli* maxipreps were performed using the Qiagen HiSpeed Plasmid Maxi Kit. Transformation of *E. coli* strains was performed using standard electroporator protocols[49]. Large amounts of linearized DNA (>20 μg), necessary for *Y. lipolytica* PO1f transformation were cleaned and precipitated using a standard phenol:chloroform extraction followed by an ethanol precipitation.

Genomic DNA (gDNA) was extracted from *Y. lipolytica* using the Wizard Genomic DNA Purification kit (Promega). Transformation of *Y. lipolytica* with episomal expression plasmids was performed using the Zymogen Frozen EZ Yeast Transformation Kit II (Zymo Research Corporation), with plating on YSC-LEU plates. Transformation of *Y. lipolytica* PO1f with linearized cassettes was performed as described previously[25], with selection on appropriate plates. Briefly, *Y. lipolytica* strains were inoculated from glycerol stock directly into 10 ml YPD media, grown overnight and harvested at an OD_{600} between 9 and 15 by centrifugation at 1,000 *g* for 3 min. Cells were washed twice in sterile water. Cells (10^8) were dispensed into separate microcentrifuge tubes for each transformation, spun down and resuspended in 1.0 ml 100 mM LiOAc. Cells were incubated with shaking at 30 °C for 60 min, spun down, resuspended in 90 μl 100 mM LiOAc and placed on ice. linearized DNA (1–5 μg) was added to each transformation mixture in a total volume of 10 μl, followed by 25 μl of 50 mg ml^{-1} boiled salmon sperm DNA (Sigma Aldrich). Cells were incubated at 30 °C for 15 min with shaking, before adding 720 μl PEG buffer (50% PEG8000, 100 mM LiOAc, pH = 6.0) and 45 μl 2 M Dithiothreitol. Cells were incubated at 30 °C with shaking for 60 min, heat-shocked for 10 min in a 39 °C water bath, spun down and resuspended in 1 ml sterile water. Cells (200 μl) were plated on appropriate selection plates. All auxotrophic or antibiotic selection markers were flanked with LoxP sites to allow for retrieval of integrated markers with the pMCS-UAS1B$_{16}$-TEF-Cre replicative vector[25].

Plasmid construction. Primer sequences can be found in the Supplementary Table 4. All *Y. lipolytica* episomal plasmids were centromeric, replicative vectors derived from plasmid pSl16-Cen1-1(227)[50] after it had been modified to include a multi-cloning site, a hrGFP green fluorescent reporter gene (pIRES-hrGFP, Agilent) driven by the strong UAS1B$_{16}$-TEF promoter[23] and a cyc1 terminator[51] to create plasmid pMCS-UAS1B$_{16}$-TEF-hrGFP. Integrative plasmids were derived from plasmids pUC-S1-UAS1B$_{16}$-Leum or pUC-S1-UAS1B$_{16}$-TEF[25] that contained 5′ and 3′ rDNA integrative sequences surrounding the following elements—(from 5′ to 3′) a uracil section marker surrounded by LoxP sites for marker retrieval, the strong UAS1B$_{16}$-Leum or UAS1B$_{16}$-TEF promoter, AscI and PacI restriction enzyme sites for gene insertion and a XPR2 minimal terminator. These integrative plasmids were also designed to contain two identical NotI restriction enzyme sites directly outside of the rDNA regions so that plasmid linearization would simultaneously remove *E. coli* pUC19-based DNA. All plasmids containing expression cassettes were sequence-confirmed before transformation into *Y. lipolytica*.

Construction of episomal expression cassettes. The following genes were PCR-amplified from *Y. lipolytica* PO1f gDNA and inserted into vector pMCS-UAS1B$_{16}$-TEF-hrGFP in place of hrGFP with an AscI/PacI digest: AMPD, ACL subunit 1 (ACL1), ACL subunit 2 (ACL2), MAE1, DGA1, and DGA2 with primers JB387/388, JB402/404, JB405/407, AH020/021, JB911/912 and JB913/914, respectively. This formed plasmids pMCS-UAS1B$_{16}$-TEF-AMPD, pMCS-UAS1B$_{16}$-TEF-ACL1, pMCS-UAS1B$_{16}$-TEF-ACL2, pMCS-UAS1B$_{16}$-TEF-MAE1, pMCS-UAS1B$_{16}$-TEF-DGA1 and pMCS-UAS1B$_{16}$-TEF-DGA2.

A leucine marker containing plasmid containing the Cre-Recombinase gene, pMCS-UAS1B$_{16}$-TEF-Cre enables constitutive, high-level Cre expression[25].

Construction of integrative expression cassettes. The following genes were gel-extracted from the previously constructed episomal expression vectors and inserted into vector pUC-S1-UAS1B$_{16}$-TEF with an AscI/PacI digest: AMPD, ACL subunit 1 (ACL1), ACL subunit 2 (ACL2), MAE1, DGA1 and DGA2. This formed plasmids pUC-S1-UAS1B$_{16}$-TEF-AMPD, pUC-S1-UAS1B$_{16}$-TEF-ACL1, pUC-S1-UAS1B$_{16}$-TEF-ACL2, pUC-S1-UAS1B$_{16}$-TEF-MAE1, pUC-S1-UAS1B$_{16}$-TEF-DGA1 and pUC-S1-UAS1B$_{16}$-TEF-DGA2. The loxP-surrounded uracil marker of these integrative plasmids was replaced with a loxP-surrounded leucine marker created

by amplification of pMCSCen1 template with primers JB862/863 followed by insertion using a BstBI/SacII digest. These plasmids enabled integrative selection with leucine auxotrophy and co-expression of two enzymes without marker retrieval. These leucine marker integrative plasmids were dubbed plasmids pUC-S2-UAS1B$_{16}$-TEF-AMPD, pUC-S2-UAS1B$_{16}$-TEF-ACL1, pUC-S2-UAS1B$_{16}$-TEF-ACL2, pUC-S2-UAS1B$_{16}$-TEF-MAE1, and pUC-S2-UAS1B$_{16}$-TEF-DGA1 and pUC-S2-UAS1B$_{16}$-TEF-DGA2.

ACL1 and ACL2 were similarly inserted into pUC-S1-UAS1B$_{16}$-Leum with primers JB403/404 and JB406/407, respectively, to form plasmids pUC-S1-UAS1B$_{16}$-Leum-ACL1 and pUC-S1-UAS1B$_{16}$-Leum-ACL2.

Strain construction. All strains were confirmed through gDNA extraction and PCR confirmation and are listed in Supplementary Table 1. We previously constructed two markerless single-gene deletion strains in the *Y. lipolytica* PO1f background, PO1f-Δmfe1 and PO1f-Δpex10, deficient in their β-oxidation and peroxisomal biogenesis capacity, respectively[25]. Following our previous protocol, the PEX10 gene was deleted from strain PO1f-Δmfe1 to form the markerless double-mutant PO1f-Δmfe1-Δpex10. These four strains, referred to as PO1f, *pex10*, *mfe1*, and *pex10 mfe1* were utilized as backgrounds for single and double overexpression of the AMPD, ACL1, ACL2, MAE1, DGA1 and DGA2 proteins, including variation in selective marker utilized, that is, leucine (chromosomal or episomal expression cassette) versus uracil (chromosomal expression cassette). Integrative cassettes were linearized, transformed into the four background strains and selected for on appropriate dropout plates. Integrative vectors without open reading frames to express, pUC-S1-UAS1B$_{16}$-TEF and pUC-S2-UAS1B$_{16}$-TEF, were utilized to create strains with leucine, uracil or both leucine and uracil prototrophies, but without enzyme overexpression (Supplementary Table 1).

Fatty-acid characterization by nile red staining. Nile red (MP Biomedicals) is commonly utilized to stain oleaginous cellular material and can be coupled with fluorescence flow cytometry to gauge relative lipid content[36]. *Y. lipolytica* strains were routinely inoculated from glycerol stock in biological triplicate in appropriate media for 72 h at 30 °C with shaking. Cell concentrations were normalized to a specific OD_{600} for reinoculation in fresh media and further incubation. For assays in which the effect of media formulation was not being investigated, this media contained 0.79 g l^{-1} CSM (or 0.69 g l^{-1} CSM-Leucine if necessary), 1.7 g l^{-1} Yeast Nitrogen Base w/o amino acid and w/o $(NH_4)_2SO_4$, 80 g l^{-1} carbon source and 5 g l^{-1} ammonium sulphate, as this formulation was shown to strongly induce lipid accumulation in the highest lipid-producing strains (Supplementary Figs 6–17). For large experiments (Figs 1 and 2), 2-ml cultures were utilized to test large number of cultures and were inoculated to an $OD_{600} = 2.5$ and larger volume cultures were inoculated to an $OD_{600} = 0.1$. Cultures were incubated for 2–8 days at 30 °C with constant agitation. Cultures (2 ml) were incubated in a rotary drum (CTλ, New Brunswick Scientific) at speed seven. Flasks were shaken at 225 r.p.m. in a standing incubator, and bioreactors were agitated by rotor at no less than 250 r.p.m. and no more than 800 r.p.m. To harvest, one OD_{600} unit of culture was spun down at 1,000 *g* for 3 minutes and resuspended in 500 µl Phosphate-Buffered Saline solution (PBS) (Sigma Aldrich). In all, 6 µl of 1 mM nile red (dissolved in DMSO) was added and then cells were incubated in the dark at room temperature for 15 min. Cells were spun down at 1000*g* for 3 minutes, resuspended in 800 µl ice cold water, spun down again and resuspended again in 800 µl ice cold water. Stained cells (300 µl) were added to 1 ml ice-cold water and tested with a FACS Fortessa (BD Biosciences), a voltage of 350, a 10,000 cell count, a forward scatter of 125, a side scatter of 125 and the 535LP and 585/42BP filters for fluorescence detection using the GFP fluorochrome. Samples were kept on ice and in the dark during the test and fluorescence data was analysed using FlowJo software (Tree Star Inc., Ashland, OR, USA) to compute mean fluorescence values. Day-to-day variability was mitigated by analysing all comparable strains on the same day. An average fluorescence and s.d. were calculated from the mean values of biological replicates. Stained cells were routinely examined with fluorescence microscopy under a ×100 oil immersion objective using the FITC channel on an Axiovert 200M microscope (Zeiss).

Lipid quantification and fatty-acid profile analysis. Lipids from a 500 µl volume of culture, or ~1.0 mg dry cell weight, were extracted following the procedure described by Folch *et al.*[52] and modified for yeast[53]. Briefly, *Y. lipolytica* cells were spun down and washed with water twice, and then resuspended in a chloroform/methanol solution (2:1) and vortexed on high with glass beads for 20 min. The organic solution was extracted and washed with 0.2 volumes of 0.3% NaCl solution before being dried at 60 °C overnight and weighed to quantify lipid production. Lipids in the culture medium were tested for, but no extracellular lipids were detected. Dry cell weight was determined after washing cells twice with H_2O and drying overnight at 60 °C. The dried lipids were transesterified with N-tert-Butyldimethylsilyl-N-methyltrifluoroacetamide (Sigma Aldrich) following the procedure of (Paik *et al.*[54]), and 2-µl samples were injected into a GC-FID (Agilent Technologies 6890 Network GC System) equipped with an Agilent HP-5 column (5% phenyl-95% methylsiloxane—product number 19091J-413) to analyse fatty-acid fractions. Briefly, the following settings were used: Detector Temp = 300 °C, He Flow = 1.0 ml min^{-1}, Oven Temp = 80 °C for 2 min, increased at 30 °C min^{-1} to 200 °C, increased at 2 °C min^{-1} to 229 °C, increased at 1 °C min^{-1} to 232 °C and increased at 50 °C min^{-1} to 325 °C. Fatty-acid standards for C16:0 palmitic acid, C16:1(n-7) palmitoleic acid, C17:0 heptadecanoic acid, C18:0 stearic acid, C18:1(n-7) oleic acid, and C18:2(n-6) linoleic acid were purchased from Sigma Aldrich, transesterified and analysed by GC to identify fatty-acid peaks. Similarly, C16:1(n-7) palmitoleic acid was purchased from Cayman Chemical and used as a standard. GC–MS confirmation of fatty acid type was performed with a Thermo Scientific TSQ Quantum Triple Quad using chemical ionization and a 1.5 ml min^{-1} flow rate. Calibration curves and comparison of GC–MS quantification and bulk extraction and GC quantification are provided in Supplementary Tables 5 and 6. Lipid quantification obtained using both methods converge within an error of <20%; thus, we determined that both methods are suitable for quantifying lipid levels in the cells.

Citric acid quantification. A 2-ml culture sample was pelleted down for 5 min at 3,000 × *g* and the supernatant was filtered using a 0.2-mm syringe filter (Corning Incorporated). Filtered supernatant was analysed with a HPLC Ultimate 3000 (Dionex) and a Zorbax SB-Aq column (Agilent Technologies). A 2.0-µl injection volume was used in a mobile phase composed of a 99.5:0.5 ratio of 25 mM potassium phosphate buffer (pH = 2.0) to acetonitrile with a flow rate of 1.25 ml min^{-1}. The column temperature was maintained at 30 °C and UV–Vis absorption was measured at 210 nm. A citric acid standard (Sigma Aldrich) was used to detect and quantify citric acid production.

Ammonium quantification. Culture (1 ml) was heated to 80 °C for 15 min, and then centrifuged at 17,900 *g* for 3 min. Supernatant was stored at 4 °C for <1 week, and ammonium concentration was determined using the R-Biopharm Ammonium Assay kit following the manufacturer's instructions. Ammonium Assay kit accuracy was assessed by measuring ammonium concentration in solutions with varying concentrations of Yeast Nitrogen Base w/o amino acids. Minor necessary adjustments were made using the resulting standard curve.

Bioreactor fermentations. Typically, bioreactor fermentations were run in minimal media (described above) as batch processes. However, one fermentation included a spike of an additional 80 g l^{-1} glucose at the 72 h timepoint, and another had a doubled media formulation that contained 160 g l^{-1} glucose and 13.4 g l^{-1} YNB w/o amino acids. All fermentations were inoculated to an initial $OD_{600} = 0.1$ in 1.5 l of media. Dissolved oxygen was maintained at 50% of maximum by varying rotor speed between 250 r.p.m. and 800 r.p.m. with a constant air input flow rate of 2.5 v v^{-1} min^{-1} (3.75 l min^{-1}). pH was maintained at 3.5 or above with 2.5 M NaOH, and temperature was maintained at 28 °C. Samples (10–15 ml) were taken every 12 hours, and fermentations lasted 6–7 days. We ran several fermentations with suboptimal conditions before settling on the above parameters.

Transesterification. *Y. lipolytica* lipid reserves were transesterified using acid-promoted direct methanolysis of cellular biomass[55]. A total of 1 l of *pex10 mfe1* leucine$^+$ uracil$^+$ DGA1p fermented in a bioreactor for 7 days as described above was washed twice in 400 ml water. Cells were dried on a hot plate at 140 °C for 3 h. The dried cell mass was transesterified with 2% w v^{-1} H_2SO_4 in 200 ml methanol at a fast boil with reflux and constant agitation for 72 h. The reaction mixture was centrifuged to remove cellular debris. FAMEs were extracted from the supernatant by adding 0.2 volumes water, mixing, centrifuging and removing the polar phase. Additional FAMEs were extracted in the polar phase with a second extraction using 0.4 volume of water. FAMEs were washed in 1 volume of water and analysed with TLC and GC.

Thin layer chromatography. A thin layer chromatography of transesterified lipid product was run on a silica gel 60 TLC plate with hexane (Fischer Scientific)—diethyl ether (Sigma Aldrich)—acetic acid (Mallinckrodt Baker, Inc) at 40:10:1 using 6 µl of 1.25 µg µl^{-1} standard mixture and 6 µl of 1 µg µl^{-1} sample and then visualized with iodine vapour (Sigma Aldrich).

Protein extraction. Protein content from 0.5–1.0 ml of culture was extracted using the Pierce BCA Protein Assay Kit following the manufacturer's instructions. Protein concentration (mg ml^{-1}) was normalized per ml of culture and per culture OD_{600} to normalize to the individual cellular level. PO1f leucine$^+$ uracil$^+$ and *pex10 mfe1* leucine$^+$ uracil$^+$ DGA1p strains were analysed in this manner after fermentation in a bioreactor.

Glucose quantification. Supernatant was diluted 1:10 and glucose concentration was quantified using a YSI Life Sciences Bioanalyzer 7100MBS.

References

1. Curran, K. A. & Alper, H. S. Expanding the chemical palate of cells by combining systems biology and metabolic engineering. *Metab. Eng.* **14,** 289–297 (2012).
2. Lee, J. W. *et al.* Systems metabolic engineering of microorganisms for natural and non-natural chemicals. *Nat. Chem. Biol.* **8,** 536–546 (2012).
3. Zhang, F. Z., Carothers, J. M. & Keasling, J. D. Design of a dynamic sensor-regulator system for production of chemicals and fuels derived from fatty acids. *Nat. Biotechnol.* **30,** 354–360 (2012).
4. Atsumi, S., Hanai, T. & Liao, J. C. Non-fermentative pathways for synthesis of branched-chain higher alcohols as biofuels. *Nature* **451,** 86–89 (2008).
5. Li, Q., Du, W. & Liu, D. H. Perspectives of microbial oils for biodiesel production. *Appl. Microbiol. Biotechnol.* **80,** 749–756 (2008).
6. Schirmer, A., Rude, M. A., Li, X. Z., Popova, E. & del Cardayre, S. B. Microbial Biosynthesis of Alkanes. *Science* **329,** 559–562 (2010).
7. Steen, E. J. *et al.* Microbial production of fatty-acid-derived fuels and chemicals from plant biomass. *Nature* **463,** 559–U182 (2010).
8. Lu, X. F., Vora, H. & Khosla, C. Overproduction of free fatty acids in *E. coli*: Implications for biodiesel production. *Metab. Eng.* **10,** 333–339 (2008).
9. Rodolfi, L. *et al.* Microalgae for Oil: Strain Selection, Induction of Lipid Synthesis and Outdoor Mass Cultivation in a Low-Cost Photobioreactor. *Biotechnol. Bioeng.* **102,** 100–112 (2009).
10. Alvarez, H. M., Mayer, F., Fabritius, D. & Steinbuchel, A. Formation of intracytoplasmic lipid inclusions by *Rhodococcus opacus* strain PD630. *Arch. Microbiol.* **165,** 377–386 (1996).
11. Dellomonaco, C., Clomburg, J. M., Miller, E. N. & Gonzalez, R. Engineered reversal of the beta-oxidation cycle for the synthesis of fuels and chemicals. *Nature* **476,** 355–U131 (2011).
12. Makri, A., Fakas, S. & Aggelis, G. Metabolic activities of biotechnological interest in *Yarrowia lipolytica* grown on glycerol in repeated batch cultures. *Bioresour. Technol.* **101,** 2351–2358 (2010).
13. Tai, M. & Stephanopoulos, G. Engineering the push and pull of lipid biosynthesis in oleaginous yeast *Yarrowia lipolytica* for biofuel production. *Metab. Eng.* **15,** 1–9 (2013).
14. Beopoulos, A. *et al.* Control of lipid accumulation in the yeast *Yarrowia lipolytica*. *Appl. Environ. Microbiol.* **74,** 7779–7789 (2008).
15. Dulermo, T. & Nicaud, J. M. Involvement of the G3P shuttle and beta-oxidation pathway in the control of TAG synthesis and lipid accumulation in *Yarrowia lipolytica*. *Metab. Eng.* **13,** 482–491 (2011).
16. Fontanille, P., Kumar, V., Christophe, G., Nouaille, R. & Larroche, C. Bioconversion of volatile fatty acids into lipids by the oleaginous yeast *Yarrowia lipolytica*. *Bioresour. Technol.* **114,** 443–449 (2012).
17. Papanikolaou, S., Chevalot, I., Komaitis, M., Marc, I. & Aggelis, G. Single cell oil production by *Yarrowia lipolytica* growing on an industrial derivative of animal fat in batch cultures. *Appl. Microbiol. Biotechnol.* **58,** 308–312 (2002).
18. Dujon, B. *et al.* Genome evolution in yeasts. *Nature* **430,** 35–44 (2004).
19. Fickers, P., Le Dall, M. T., Gaillardin, C., Thonart, P. & Nicaud, J. M. New disruption cassettes for rapid gene disruption and marker rescue in the yeast *Yarrowia lipolytica*. *J. Microbiol. Methods* **55,** 727–737 (2003).
20. Juretzek, T. *et al.* Vectors for gene expression and amplification in the yeast *Yarrowia lipolytica*. *Yeast.* **18,** 97–113 (2001).
21. Fournier, P. *et al.* Colocalization of centromeric and replicative functions on autonomously replicating sequences isolated from the yeast *Yarrowia lipolytica*. *Proc. Natl Acad. Sci. USA* **90,** 4912–4916 (1993).
22. Blazeck, J. *et al.* Generalizing a hybrid synthetic promoter approach in *Yarrowia lipolytica*. *Appl. Microbiol. Biotechnol.* **97,** 3037–3052 (2013).
23. Blazeck, J., Liu, L., Redden, H. & Alper, H. Tuning gene expression in *Yarrowia lipolytica* by a hybrid promoter approach. *Appl. Environ. Microbiol.* **77,** 7905–7914 (2011).
24. Liu, L., Redden, H. & Alper, H. Frontiers of yeast metabolic engineering: diversifying beyond ethanol and *Saccharomyces*. *Curr. Opin. Biotechnol.* **24,** 1023–1030 (2013).
25. Blazeck, J., Liu, L., Knight, R. & Alper, H. Heterologous production of pentane in the oleaginous yeast *Yarrowia lipolytica*. *J. Biotechnol.* **165,** 184–194 (2013).
26. Beopoulos, A. *et al. Yarrowia lipolytica* as a model for bio-oil production. *Prog. Lipid Res.* **48,** 375–387 (2009).
27. Barth, G. & Gaillardin, C. in *Nonconventional Yeasts in Biotechnology: A Handbook* Vol. 1 (ed Wolf, K.) ch 10, 313–388 (Springer, 1996).
28. Zhang, H. *et al.* Regulatory properties of malic enzyme in the oleaginous yeast, *Yarrowia lipolytica*, and its non-involvement in lipid accumulation. *Biotechnol. Lett.* **35,** 2091–2098 (2013).
29. Rodríguez-Frómeta, R. A., Gutiérrez, A., Torres-Martínez, S. & Garre, V. Malic enzyme activity is not the only bottleneck for lipid accumulation in the oleaginous fungus *Mucor circinelloides*. *Appl. Microbiol. Biotechnol.* **97,** 3063–3072 (2013).
30. Vorapreeda, T., Thammarongtham, C., Cheevadhanarak, S. & Laoteng, K. Alternative routes of acetyl-CoA synthesis identified by comparative genomic analysis: involvement in the lipid production of oleaginous yeast and fungi. *Microbiology* **158,** 217–228 (2012).
31. Caspi, R. *et al.* The MetaCyc database of metabolic pathways and enzymes and the BioCyc collection of pathway/genome databases. *Nucleic Acids Res.* **40,** D742–D753 (2012).
32. Sherman, D. *et al.* Génolevures complete genomes provide data and tools for comparative genomics of hemiascomycetous yeasts. *Nucleic Acids Res.* **34,** D432–D435 (2006).
33. Xue, Z. *et al.* Production of omega-3 eicosapentaenoic acid by metabolic engineering of *Yarrowia lipolytica*. *Nat. Biotechnol.* **31,** 734–740 (2013).
34. Beopoulos, A. *et al.* Identification and characterization of DGA2, an acyltransferase of the DGAT1 acyl-CoA:diacylglycerol acyltransferase family in the oleaginous yeast *Yarrowia lipolytica*. New insights into the storage lipid metabolism of oleaginous yeasts. *Appl. Microbiol. Biotechnol.* **93,** 1523–1537 (2012).
35. Hong, S., Sharpe, P., Xue, Z., Yadav, N. & Zhu, Q. Peroxisome biogenesis factor protein (pex) disruptions for altering the content of polyunsaturated fatty acids and the total lipid content in oleaginous eukaryotic organisms. 12/244,950 USA patent (2008).
36. Greenspan, P., Mayer, E. P. & Fowler, S. D. Nile red: a selective fluroscent stain for intracelluluar lipid droplets. *J. Cell Biol.* **100,** 965–973 (1985).
37. Ratledge, C. Regulation of lipid accumulation in oleaginous micro-organisms. *Biochem. Soc. Trans.* **30,** 1047–1050 (2002).
38. Jimenez-Marti, E. *et al.* Molecular response of *Saccharomyces cerevisiae* wine and laboratory strains to high sugar stress conditions. *Int. J. Food Microbiol.* **145,** 211–220 (2011).
39. Botham, P. A. & Ratledge, C. A biochemical explanation for lipid accumulation in *Candida* 107 and other oleaginous micro-organisms. *J. Gen. Microbiol.* **114,** 361–375 (1979).
40. Evans, C. T. & Ratledge, C. Biochemical activities during lipid accumulation in *Candida curvata*. *Lipids* **18,** 630–635 (1983).
41. Evans, C. T., Scragg, A. H. & Ratledge, C. A comparative study of citrate efflux from mitochondria of oleaginous and non-oleaginous yeasts. *Eur. J. Biochem.* **130,** 195–204 (1983).
42. Atkinson, B. M. F. *Biochemical Engineering and Biotechnology Handbook.* 120 (Palgrave Macmillan, 1983).
43. Hammond, E. G., Johnson, L. A., Su, C., Wang, T. & White, P. J. in *Bailey's Industrial Oil and Fat Products* (ed. Shahidi, F.) Ch 13, 577–653 (John Wiley & Sons, Inc., 2005).
44. Laplante, M. & Sabatini, D. M. An emerging role of mTOR in lipid biosynthesis. *Curr. Biol.* **19,** R1046–R1052 (2009).
45. Sancak, Y. *et al.* The Rag GTPases bind raptor and mediate amino acid signaling to mTORC1. *Science* **320,** 1496–1501 (2008).
46. Han, J. M. *et al.* Leucyl-tRNA synthetase is an intracellular leucine sensor for the mTORC1-signaling pathway. *Cell* **149,** 410–424 (2012).
47. Bonfils, G. *et al.* Leucyl-tRNA synthetase controls TORC1 via the EGO complex. *Mol. Cell* **46,** 105–110 (2012).
48. Madzak, C., Treton, B. & Blanchin-Roland, S. Strong hybrid promoters and integrative expression/secretion vectors for quasi-constitutive expression of heterologous proteins in the yeast Yarrowia lipolytica. *J. Mol. Microbiol. Biotechnol.* **2,** 207–216 (2000).
49. Sambrook, J. & Russell, D. W. *Molecular Cloning* 1.119 (CSHL Press, 2001).
50. Yamane, T., Sakai, H., Nagahama, K., Ogawa, T. & Matsuoka, M. Dissection of centromeric DNA from yeast *Yarrowia lipolytica* and identification of protein-binding site required for plasmid transmission. *J. Biosci. Bioeng.* **105,** 571–578 (2008).
51. Mumberg, D., Muller, R. & Funk, M. Yeast vectors for the controlled expression of heterologous proteins in different genetic backgrounds. *Gene* **156,** 119–122 (1995).
52. Folch, J., Lees, M. & Stanley, G. H. S. A simple method for the isolation and purification of total lipids from animal tissues. *J. Biol. Chem.* **226,** 497–509 (1957).
53. Schneiter, R. & Daum, G. Extraction of yeast lipids. *Methods Mol. Biol.* **313,** 41–45 (2006).
54. Paik, M.-J., Kim, H., Lee, J., Brand, J. & Kim, K.-R. Separation of triacylglycerols and free fatty acids in microalgal lipids by solid-phase extraction for separate fatty acid profiling analysis by gas chromatography. *J. Chromatography A* **1216,** 5917–5923 (2009).
55. Liu, B. & Zhao, Z. Biodiesel production by direct methanolysis of oleaginous microbial biomass. *J. Chem. Technol. Biotechnol.* **82,** 775–780 (2007).

Acknowledgements

This work was funded by the Office of Naval Research Young Investigator Program, the DuPont Young Professor Grant and the Welch Foundation under grant F-1753. We would like to thank Masayoshi Matsuoka for the gift of plasmid pSl16-Cen1-1(227). We would like to thank Alex Voice, Paul Nielsen, Nathan Fine and Gary Rochelle for assistance with and access to an HPLC. We would like to thank David Nobles for assistance with FLM.

Author contributions

J.B., A.H. and L.L. performed all the experiments. J.B. and A.H. generated POIf derivatives. J.B., A.H., L.L., J.M., A.P. and PO created expression cassettes. L.L. extracted lipid products and R.K. analysed fatty-acid profiles with GC/GC–MS. A.H. performed transesterification reactions. J.B., L.L. and H.S.A. designed experiments. J.B. and H.S.A. conceived of experiments and wrote the manuscript.

Additional information

Supplementary Information accompanies this paper at http://www.nature.com/naturecommunications

Competing financial interests: J.B., A.H., L.L. and H.A. have filed a provisional patent in 2013 "Compositions and methods for fungal lipid production" relating to the strains and techniques developed in this study. The remaining authors declare no competing financial interests.

Reprints and permission information is available online at http://npg.nature.com/reprintsandpermissions/

How to cite this article: Blazeck, J. *et al.* Harnessing *Yarrowia lipolytica* lipogenesis to create a platform for lipid and biofuel production. *Nat. Commun.* 5:3131 doi: 10.1038/ncomms4131 (2014).